

Wavefront-Based Models for Inverse Electrocardiography

Alireza Ghodrati*, *Member, IEEE*, Dana H. Brooks, *Senior Member, IEEE*, Gilead Tadmor, *Senior Member, IEEE*, and Robert S. MacLeod, *Member, IEEE*

Abstract—We introduce two wavefront-based methods for the inverse problem of electrocardiography, which we term wavefront-based curve reconstruction (WBCR) and wavefront-based potential reconstruction (WBPR). In the WBCR approach, the epicardial activation wavefront is modeled as a curve evolving on the heart surface, with the evolution governed by factors derived phenomenologically from prior measured data. The body surface potential/wavefront relationship is modeled via an intermediate mapping of wavefront to epicardial potentials, again derived phenomenologically. In the WBPR approach, we iteratively construct an estimate of epicardial potentials from an estimated wavefront curve according to a simplified model and use it as an initial solution in a Tikhonov regularization scheme. Initial simulation results using measured canine epicardial data show considerable improvement in reconstructing activation wavefronts and epicardial potentials with respect to standard Tikhonov solutions. In particular the WBCR method accurately finds the anisotropic propagation early after epicardial pacing, and the WBPR method finds the wavefront (regions of sharp gradient of the potential) both accurately and with minimal smoothing.

Index Terms—Electrocardiography, inverse electrocardiography, inverse problem, Kalman filter, regularization, state evolution model.

I. INTRODUCTION

INVERSE electrocardiography is a noninvasive imaging method to reconstruct the heart's electrical activity from remote surface measurements. Recent reports indicate great potential for this imaging modality to be used in clinical practice for cardiac electrophysiology and arrhythmias [1], [2]. Approaches to inverse electrocardiography have generally relied on either an activation-based model or a surface potential-based model (using epicardial, endocardial, or trans-membrane potentials) [3]–[12]. Activation-based models reduce the unknowns to the arrival time of the wavefront at each point on the epicardial and endocardial surfaces. Potential-based models, in contrast, treat the value of the potential at each point on the relevant surface, or in the myocardium at each time instant, as a free variable. Thus, activation-based models are low-order parameterizations which capture the single most

important physiological feature of cardiac propagation, while potential-based models are high-order parameterizations which can accommodate a broad range of possible phenomena.

In particular, activation-based models typically make isotropy/homogeneity assumptions and use a fixed shape of the temporal waveforms [3], [4], [6], for several reasons. For one, details of the specifics of anisotropic organization of the myocardium of a given individual may be difficult to acquire. Secondly, it is to date not completely clear how important these factors are in inverse solution accuracy [13]. Perhaps most significantly, at least historically, these assumptions allow a more tractable source model and forward model. Thus, activation-based methods may not take advantage of all information about cardiac sources which is available in the measurements, nor of known prior information about anisotropic conduction and the true three-dimensional (3-D) nature of wavefront propagation. For instance, in [14] and [15], features such as diminished height of the wavefront and decreased slope of the intrinsic deflection in areas of infarction, and even electrogram waveforms showing mixed characteristics in the infarct border zone, were all approximately reconstructed using a potential-based approach. Moreover, as pointed out in [11] and [16], potential-based reconstructions may be better able to address settings such as postinfarction when the spatially constant waveform assumption of activation-based methods may not apply.

Despite their simplifying assumptions, activation-based methods are ill-posed—solutions are overly sensitive to normal levels of noise and model error and need regularization, and/or a well-posed initial estimate [5], to obtain a meaningful inverse solution. However, they are considerably better posed, and require less explicit regularization, than potential-based models, due to the implicit regularization effect of the fixed waveform shape, and have been reported to be notably more robust with respect to errors in the geometry or to measurement noise [17]. The less restrictive nature of potential-based models, with their high-order parameterization, gives rise to a much more ill-posed inverse problem which requires considerable smoothing (regularization). Moreover these minimally restricted formulations do not easily lend themselves to the inclusion of the physical and geometric constraints implied by the central physiological feature of cardiac propagation, namely wavefront behavior, except via indirect and somewhat coarse models [7], [11].

It would, therefore, seem useful to pursue models that seek to leverage the advantages and address the shortcomings of both approaches. Such models should try to maintain the low dimensionality implied by a focus on wavefront behavior, but should relax the isotropy and homogeneity assumptions of activation

Manuscript received August 1, 2005; revised February 9, 2006. This work was supported in part by the Center for Integrative Biomedical Computing, NIH NCRN Project 2-P41-RR12553-07. *Asterisk indicates corresponding author.*

*A. Ghodrati is with the Department of Algorithm Development, Draeger Medical, Andover, MA 01810 USA (alireza.ghodrati@draeger.com)

D. H. Brooks and G. Tadmor are with the Communications and Digital Signal Processing Center, Department of Electrical and Computer Engineering, Northeastern University, Boston, MA 02115 USA.

R. S. MacLeod is with the Nora Eccles Harrison Cardiovascular Research and Training Institute (CVRTI), University of Utah, Salt Lake City, UT 84112 USA.

Digital Object Identifier 10.1109/TBME.2006.878117

models, and should also seek to permit inclusion of relevant physiology and electrophysiology. We propose here two such approaches as initial progress in this direction. We call these two approaches wavefront-based curve reconstruction (WBCR) and wavefront-based potential reconstruction (WBPR). We present the results of simulations using these methods only for epicardial potentials, but we discuss the possibility of using other source models as well.

In the WBCR approach we formulate the inverse problem in terms of the temporal evolution of the activation wavefront, using a data-based predetermined function to predict the epicardial potentials from the wavefront location. In particular, the quantity that we reconstruct is a low-order parameterization of the wavefront location. The wavefront evolves in the normal direction over time according to a second function which incorporates a data-based predetermined velocity model. A state evolution approach is used to drive the wavefront propagation from the measurements. Initial results of this approach were reported in [18]. In the WBPR approach, our focus shifts to reconstruction of the potentials, but the solution of the associated inverse problem exploits an explicit approximation of wavefront behavior, based on a simplified potential model, to determine a prior estimate used as a regularizing term. The body surface measurements are used to update the prior estimates via the solution of a structured inverse problem; the update of the prior aims to minimize the regularized squared error of the measurement residual. The time step is completed with an *a posteriori* estimate of the wavefront, as determined from the updated potential estimates. The WBPR approach applies its predetermined potential model in a less strict way than the WBCR approach applies its potential model, striking a compromise between its prediction, or initial estimate, and minimization of a residual.

In this initial report, we concentrate on paced beats initiated by a stimulus on the epicardium. Due to the relative geometric and physiological simplicity of the ensuing propagation, this is the simplest case for this model. However we report also on a test of the WBPR approach for a supraventricularly paced heart-beat, and discuss the challenges and potential solutions for wider applicability of each method.

II. METHOD I: WAVEFRONT-BASED CURVE RECONSTRUCTION (WBCR)

This section explains our first approach, in which the problem is formulated in terms of reconstruction of the activation wavefront curve. Highlights of the WBCR approach include the following.

- 1) The model is focused on the evolution of the wavefront on the epicardial surface.
- 2) The predicted temporal evolution of each wavefront node, at each time instant, is in the direction normal to the curve, according to a predetermined velocity function.
- 3) As with activation models, the potentials on the heart surface are fixed based on the wavefront location. The body surface potentials are modeled by a standard potential-to-potential forward solution.

- 4) The parameters that determine the velocity function and the fixed wavefront-to-potential function are chosen phenomenologically by fitting to measured data.
- 5) The combination of a simple, predetermined potential model with the potential-based forward model inevitably leads to errors in the resulting wavefront-based forward model. We use a dynamic observer (an extended Kalman filter (EKF) [19]) in the inverse solution to address this error. The EKF invokes the combined forward model and the postulated dynamic model of the wavefront; the wavefront defines the (unknown) *state* of the system, and the instantaneous body surface measurements provide spatio-temporal data.

A. State-Space Model

The basis of our proposed model is the idea that the wavefront, conceived of as a curve on the epicardial surface, is sufficient to determine the concurrent distributed potentials on the body surface, at least to within a reasonable level of uncertainty. In particular, we treat the wavefront as the *state* of the system. Our goal is to derive a state space model for the time evolution of the curve, and then to exploit a state-space method to dynamically estimate the curve. The state is a continuous curve in an infinite-dimensional function space, treated computationally via a low-order parameterization of the curve.

The WBCR model equations are

$$\begin{cases} c_{n+1} = f(c_n) + u_{n+1} \\ y_{n+1} = Ag(c_{n+1}) + w_{n+1} \end{cases} \quad (1)$$

where subscript n represents the time instant, c is the curve representing the wavefront, y is an $M \times 1$ vector holding torso potentials, A is an $M \times N$ matrix representing the forward model, f is the state evolution function, g is a function that returns the epicardial potentials from the activation wavefront curve, and u and w are Gaussian white noise variables that represent the temporal model error and forward problem error, respectively: $w_n \sim N(0, C_n)$ and $u_n \sim N(0, Q_n)$. The most crucial part of building the model is finding appropriate functions f and g , as we describe in the next section.

B. Model Elements

1) *State Evolution Function:* The function f in (1) models the propagation of the activation wavefront in time as a function of the parameterized wavefront curve. It returns a parametrization of an estimate of the wavefront curve at the next time instant, and should reflect to the extent reasonable the behavior of the 3-D myocardium.

To determine the function f , i.e., evolving the curve on the heart surface, requires a model of the apparent velocity as visible on the epicardium in the normal direction, at each point of the curve, at each time instant. Based on studies reported below of a number of canine heartbeats provided by our collaborators at the Cardiovascular Research and Training Institute (CVRTI), and in accordance with the observations reported in [20], [21], we postulated the following rules for the wavefront speed model: 1) The local fiber direction dominates other factors early after activation in a manner proportional to the projection

of that direction onto the normal direction to the curve. 2) The normal propagation velocity increases with time, and eventually becomes essentially isotropic. 3) The propagation velocity depends on the location on the epicardium, e.g., with faster propagation over the apex and the right ventricle, and lower speed over the septum.

Based on these properties we modeled the speed as follows:

$$v(s, t) = \gamma(s) (a(t) \cos^2(\eta) + b(t)) \quad (2)$$

where $v(s, t)$ is the wavefront speed at location s on the activation wavefront at time t after initiation, $\gamma(s)$ models spatial factors, η is the angle between the normal direction to the wavefront and the local fiber direction at s (which we assume is known—later we discuss how we obtain it in the experiments reported here), and a and b are coefficients of the fiber direction effect. Hence, the speeds at time t along (and across) the fibers are proportional to $a(t) + b(t)$ (and $b(t)$), respectively. The function f , then, in (1), evolves the wavefront curve c at each time instant on the heart surface by moving all points on curve in the normal direction according to the speed function $v(s, t)$ evaluated for $s \in c$.

2) *Potential Model*: The potential function g determines the potential value at each point on the heart using the wavefront curve information. This function is based on dividing the epicardial surface into three regions: activated, inactive and a transition region near the wavefront curve. The potential model also depends on the increasing trend in the time-varying reference (using the Wilson Central Terminal or an equivalent), as documented in [22]. The potential of the activated and inactive regions are assumed to be a (known) negative constant and zero, plus the time-varying reference potential, respectively. To determine the relation between potentials and wavefront curve (and, thus, the function g), we assume that the potential at each point s on the heart surface is a one-dimensional function Γ of the distance $d(s)$ of the point from the wavefront curve c , $d(s) = \min_c \|s - c\|_2$

$$\Gamma(s) = \alpha \frac{V}{2} \left(1 - \frac{1}{\sqrt{1 - \xi^2}} e^{-\xi \omega d} \sin(\omega \sqrt{1 - \xi^2} d + \psi) \right) - \frac{V}{2} + V_{\text{ref}_k}$$

$$\alpha(s) = \begin{cases} -1 & s \text{ is in the activated region} \\ 1 & s \text{ is in the inactive region} \end{cases} \quad (3)$$

This parametrization of the potential Γ is based on the form of the step response of a second-order linear system, with $d(s)$ substituting for the time variable: Here, $\omega > 0$ and $\xi \in (0, 1)$ control the slope and overshoot (undershoot) of the potential function, $\psi = \arctan(\sqrt{1 - \xi^2}/\xi)$, V is the wavefront height, and V_{ref_k} represents the reference potential at time instant k .

Fig. 1 contains plots of Γ as a function of the distance d for points outside the wavefront (i.e., $\alpha = 1$), with $V = 20$ mV and for different values of ω and ξ , when V_{ref_k} is zero. Ahead of the wavefront curve, the potential saturates to zero, while for points inside the curve there is a symmetric trend to saturation at $-V$. The selection of the values of ω and ξ are significant in the transition region, and the postulated parametrization of Γ

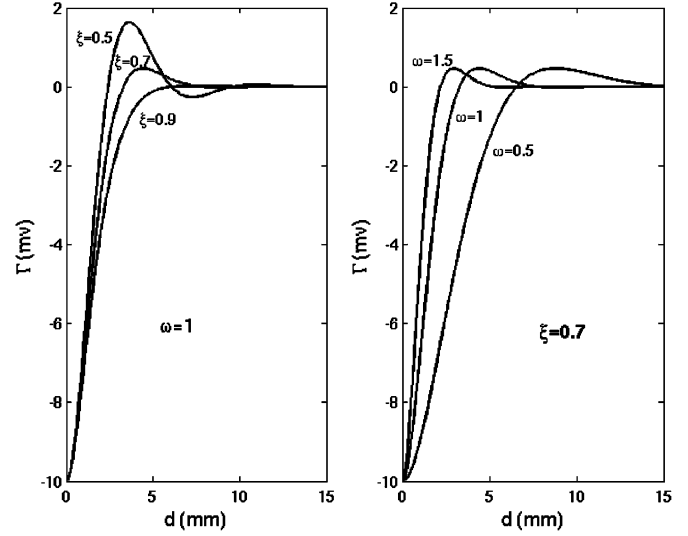


Fig. 1. Function Γ versus distance d for different values of ξ and ω .

provides flexibility to determine the slopes and overshoot or undershoot at different locations of the wavefront curve. We note that the over/under shoot capability is included to allow us to model important, if secondary, anisotropic phenomena such as the positive maxima which precede the arrival of the wavefront and the negative minima which follow it, as described in [21].

As we describe in detail below, our studies of canine epicardial data showed a weak correlation between the parameters of Γ and both fiber directions and time. By fitting the parameters ω and ξ to these data, we predefined Γ as a function of distance, fiber directions and time. We note that we could achieve increased flexibility if we were to include selected parameters of Γ in the state variables and estimated them using the body surface measurements.

At each time instant, the function g in (1) returns a vector holding the potentials at all the points s in the geometrical model of the heart surface. The values returned by g are found by first finding $d(s)$ for each point s , as described later, and then setting the potential at s by evaluating $\Gamma(d(s))$.

C. Filtering the Residual

The estimate of the state-space model at each time instant in the EKF algorithm is a combination of a prediction term based on the estimate at the previous time instant, and a correction term that depends on the current measurements via minimization of the residual norm $\|y_n - Ag(c_n)\|$. Because our model makes the simplifying assumptions of constant potential in the activated and inactive regions and a simple profile in the transition region, a systematic error is expected in the predicted body surface measurements $Ag(c_n)$, even if the wavefront curve c were to be located at the *true* location [23]. Thus, minimizing the residual may fit this error in the potential model rather than the error in the wavefront location. Examination of empirical data revealed that the error on the body surface potentials caused by this epicardial potential surface model error generally had low spatial frequency content; indeed, we found that this model error was well matched to the low-order left singular vectors of the forward matrix A [23]. To attenuate the effect of this error, then,

we simply removed the projection of the residual onto the first k left singular vectors of A before using the residual in the EKF. Formally, if the singular value decomposition of A is written $A = U\Sigma V^T$, then we formed the matrix U_k from columns $k+1$ to N of U , and the filtered residual was

$$U_k^T (y_n - Ag(c_n)). \quad (4)$$

The order of the filter, k , is an important factor which was determined empirically from the simulations described later.

D. Implementation

To find the parameters of our model we used 12 canine heartbeats, 6 paced on the left ventricle and 6 on the right ventricle, provided from previously acquired experimental data at CVRTI (details in Section IV). Pacing locations were in different regions (middle, apical, basal) of the epicardium. Since we did not have fiber information for these animals, and to ensure that our model was not overly dependent on accurate determination of fiber directions, the Auckland heart epicardial surface fiber directions [24] were used, after suitable geometry matching, to approximate fiber directions on the surface of our experimental heart. This geometry matching consisted of a rigid body fit to a single generic representation of all the hearts used in the CVRTI experiments. After matching we verified that it was reasonably accurate by visually comparing the matched directions to the spread of activation induced by epicardial pacing on a large number of experimental beats from many animals, and found good agreement.

The reference drift was removed from the experimental data by using the electrogram of the first and last activated nodes, based on the assumption that the true (constant-reference) potential of the first-activated node should be negative and constant after activation, and that of the last-activated node should be zero (and constant) until activation [25]. Thus, the time variation of the potential of the last-activated lead was used to determine the reference drift during the first half of the QRS, and the difference between the measured value at the first-activated lead and the negative activation value of the reference-corrected potentials in the activated area was used in the second half of QRS. We note that this same approach was used in [26] for propagation simulations. A different but essentially equivalent approach was used in [25] with experimental data.

We defined the activation wavefront as those points on the heart surface whose potentials were at 0.5 of the (constant, reference-removed) negative value of the activated region (i.e., the midpoints of the wavefront wall), based on a linear interpolation over the surface. (Note that here we used a spatial rather than temporal definition of activation, as suggested in [27].) The resulting curve is an estimate of the activation isochrone at each time instant. Evolving wavefronts were computed for all 12 beats. The local normal direction and velocity were then estimated at each node. The results of this study are discussed in Section IV.

To implement the state space model, the wavefront must be represented as a continuous curve evolving on the heart surface.

To force the wavefront curve to stay on the irregular triangulated geometry used to represent the heart, points on the curve were expressed in a spherical coordinate system with parameters θ and ϕ . For any given θ and ϕ , the radius r was obtained by linear interpolation of the heart surface, i.e., linear interpolation of the value $r(\theta, \phi)$, using the known value of r at the heart surface nodes. We shifted and rotated the coordinate system so that the major heart axis coincided with the positive x axis to prevent discontinuity in the azimuth angle (θ). The wavefront curve was parameterized via cubic B-spline interpolation of a number of points, starting at 5 points at the beginning of QRS and adding an additional point each 4 ms. Each time a point was added to the spline representation the points were then redistributed uniformly around the curve. By using this discrete representation of the underlying continuous curve, we were able to increase the number of points used to represent the curve without violating the state-space paradigm which requires that the dimension of the state space (here, infinite) stay fixed. The dimensions of the matrix used to represent the error covariance of the state variables, as parameterized through the discretization, did change, which was implemented by a simple interpolation scheme.

We used (2) to implement the function f . This function moved each point of the wavefront curve along the curve's normal direction in the tangential plane to the heart surface at the point. The radius, r , of the resultant curve points were then adjusted to remain on the heart surface. For simplicity, in this initial report we set $a(t) = .6$, $b(t) = .3$, and $\gamma = 1$ in (2). We implemented function g based on (3). For this purpose we needed to find the distance from each point on the heart surface to the wavefront curve. Calculation of an accurate distance from all the points on the heart surface to the wavefront could be time consuming; however, great accuracy was not required, especially for the points far from the curve since their potential was close to constant. Therefore, we approximated the path between any two points as being on a sphere whose center was at the center of the heart and whose radius was the average of the distances of the two points from that center. We approximated the center as the mean location of the surface nodes. This spherical arc approximation of the distance is obviously more accurate for the points close to the curve and less accurate for those far from the curve, just as required by our model. We used 60 points on the underlying wavefront curve to find $d(s)$, approximated as the minimum distance from each surface point s to the curve points.

We also needed to determine if a point on the heart surface was inside or outside of the wavefront curve, to set the value of α in (3). For this purpose we simply mapped the curve to a 2-D plane with the θ and ϕ axes as the Cartesian coordinates (thus preserving the topology) and then calculated the total rotation of a line between each node and the wavefront curve while the end on the wavefront circumnavigated the curve. If the point was inside the curve, this rotation was 2π , otherwise it was zero.

We used the 12 measured canine beats described earlier to determine the parameters ω and ξ of the potential model, which we set as $\omega = .7$ and $\xi = .7/\cos^2(\eta) + .5$. The EKF algorithm was implemented to solve the state-space model, linearizing the functions f and g at each time step using a finite difference method.

III. METHOD II: WAVEFRONT-BASED POTENTIAL RECONSTRUCTION (WBPR)

The second method, in which the quantities to be reconstructed were the epicardial potentials, again employed a wavefront-based model of the epicardial potentials as a two level “image,” with relatively sharp boundaries and an interpolated transition region. However, here this two-level model was used as an initial estimate, or prior mean, and then updated using the body surface measurements. As before, after subtraction of the time-varying reference in the model, the activated region was set at a negative potential, the inactivate region at zero potential, and the transition region was defined to follow a simple, relatively sharp profile. The reference potential drift, which shifts this two level image, increasing over time proportionally to the area of the activated region [25], was again modeled explicitly. From the boundary location and the two levels of the image, the model constructed a crude initial estimate of the potentials.

Specifically, to obtain this estimate we used a wavefront-based model of the transition profile which was similar but less complicated than the one used in the WBCR method

$$\bar{x}_{k,i} = \alpha_{k,i} \frac{V}{2} (1 - e^{-0.5d_{k,i}}) - \frac{V}{2} + V_{\text{ref}_k} \quad (5)$$

where $\bar{x}_{k,i}$ is the potential estimate of the i th node at time instant k , $\alpha_{k,i}$ is -1 or 1 depending on whether the i th node is inside or outside the wavefront, respectively, V is the wavefront height ($V = 20$ mV), $d_{k,i}$ is the distance of the i th node to the wavefront curve at time instant k , and V_{ref_k} is the potential reference at time instant k . The wavefront at time k is defined as the contour at a potential of the average of the two levels, $(-V + V_{\text{ref}_k})/2$.

The idea behind the WBPR method is to use this initial wavefront-based potential estimate as a constraint on the inverse solution. We did so by using this initial estimate as an initial solution in a deterministic Tikhonov regularization. (We discuss a statistical interpretation of the method below.) The Tikhonov (sometimes called Twomey) [28] solution in the presence of an initial estimate at time instant k , was obtained by minimizing

$$J_k = \|\mathbf{A}\mathbf{x}_k - \mathbf{y}_k\|_2^2 + \lambda^2 \|\mathbf{x}_k - \bar{\mathbf{x}}_k\|_2^2 \quad (6)$$

where \mathbf{y}_k are the potential measurements on the torso at time instant k , \mathbf{A} is the forward matrix, \mathbf{x}_k holds the heart surface potentials at time instant k , λ is the regularization parameter, and $\bar{\mathbf{x}}_k$ is the initial wavefront-based estimate.

The inverse solution obtained from the minimization of J_k follows:

$$\hat{\mathbf{x}}_k = \bar{\mathbf{x}}_k + (\mathbf{A}^T \mathbf{A} + \lambda^2 \mathbf{I})^{-1} \mathbf{A}^T (\mathbf{y}_k - \mathbf{A} \bar{\mathbf{x}}_k). \quad (7)$$

Viewed as a spatial-temporal process, a wavefront contour estimated from the previous time instant’s potential was used to calculate the initial wavefront-shaped model of the potentials at the current time instant. This zeroth-order predictor was used because the high temporal sampling rate of the epicardial

potentials (typically 1 kHz) meant that the wavefront position changed relatively slowly from one time sample to the next. (Typically, apparent velocities as visible on the epicardial surface are in the order of 5 mm/ms [20]). Thus, the inverse solution $\hat{\mathbf{x}}_k$ could be obtained in a temporally recursive fashion as follows:

$$\begin{aligned} \text{Step 1)} \quad & \mathbf{c}_k = \mathbf{h}(\hat{\mathbf{x}}_{k-1}) \\ \text{Step 2)} \quad & \bar{\mathbf{x}}_k = \mathbf{g}(\mathbf{c}_k) \\ \text{Step 3)} \quad & \text{Calculate } \hat{\mathbf{x}}_k \text{ using (7)}. \end{aligned} \quad (8)$$

where k is the time instant, \mathbf{c}_k is an interpolated continuous curve representing the wavefront, $\mathbf{h}()$ finds this wavefront curve by thresholding the potential and then using cubic B-splines to smooth the threshold contour, and $\mathbf{g}()$ is the potential function of (5).

We note that we can run this recursion backwards in time in a second pass, or alternatively forward and backward in any desired progression. We can use a similar procedure to iterate at a single time instant, starting from some initial estimate of the potentials, with k now representing the iteration number.

A. Implementation

As noted above, to start the method we need:

- the value of the reference at each time instant;
- the negative value of the activated region of some time instant and the height of the wavefront;
- an initial guess of the wavefront.

We obtained these values as follows:

In the results presented, we simply used the true negative potential of the activated region. However, based on results of other groups (e.g., [14] and [15]) as well as our own work, it should be possible to estimate this value with reasonable accuracy using a Tikhonov solution at a node far from the wavefront. The reference potential at the beginning was assumed to be zero (a correct assumption for early in QRS), and it was then extracted sequentially from the inverse solution at each time instant to be used for the next time instant. As in the WBCR method, we used the potential of the last lead to be activated as the reference drift in the first half of the QRS interval and the shift of the earliest activating node potential from its starting point as the reference drift in the second half. The initial estimate at the first time instant was taken as a circular wavefront centered at the pacing node, with a radius of about 2 cm. We assumed this pacing node was known in the simulations presented here, but again there is evidence to suggest that it could be obtained reliably enough for this purpose (with around 2 cm uncertainty) by a standard Tikhonov solution or perhaps a GMRES approach [10].

We implemented the algorithm as described in (8). A threshold function $\mathbf{h}()$ was designed to create the wavefront curve from the current estimate of the epicardial potentials. For this purpose we checked all the triangles of the heart surface triangular mesh¹ to see if they contained the wavefront. We then linearly interpolated the potentials on the sides of the triangles containing the wavefront to approximate the wavefront crossings on the sides of those triangles. This way we obtained

¹The heart surface was discretized by 490 nodes and a triangular mesh was used to represent the surface [29].

a pair of points on the wavefront on two sides of each triangle through which the wavefront passed. Neighboring triangles which contained the wavefront each shared one of these points. Thus, we started from an arbitrary pair of points and sought its neighboring pair. We continued this procedure until we reached the starting point. We also checked for multiple wavefront curves, using the above procedure to locate all of them. Finally, we downsampled the curve points and used a cubic B-spline basis to interpolate the wavefront curve or curves. Function $g(\cdot)$ was implemented based on (5) and the distance from node i to the wavefront, $d_{k,i}$, was approximated as explained in Section II-D.

In summary, at each time instant we found the wavefront corresponding to the threshold potential solution of the previous time instant, smoothed by a cubic B-spline fit, then used this smoothed wavefront to create an initial estimate for the current time instant, as explained above. This initial estimate was then used as the constraint in a Tikhonov solution as per (7). We also implemented this iterative method in the backward temporal direction. In the backward iteration we used the estimated solution at the final time instant obtained in the forward iteration as the initial solution and sequentially estimated the solutions at all preceding time instants.

IV. RESULTS

To both estimate the required model parameters and then to test both inverse solution methods, we used epicardial potentials measured from canine hearts that had been placed in a tank built to simulate an adolescent human torso at the CVRTI. Measurements were taken at 490 sites on the heart surface using a sock electrode as described elsewhere [29]. We used the boundary-element method to calculate a forward matrix based on the geometry of the heart and torso. The number of nodes on the torso mesh was 771 and, thus, the full forward matrix \mathbf{A} was 771×490 . Testing of the methods was always performed on data from different animals than those used to estimate the model parameters. In addition, as noted above, the fiber geometry, where used, came from yet another animal, and from experiments at a different laboratory. For testing the inverse solutions we simulated torso measurements from the measured heart data using the forward matrix and then added white Gaussian noise at an SNR of 30 dB.

A. Results of the WBCR Approach

We approximated the speed of the wavefront at different time instants and different nodes on the heart surface for 12 heartbeats as explained in Section II-D. We then studied the speed versus time and speed versus the cosine of the angle η between the normal direction at a point of the wavefront and the fiber direction at that point. Fig. 2(a) shows the speed versus cosine η for left ventricular paced beats, where each panel shows a different time interval of the QRS. As the results show, the speed of the wavefront is higher along the fiber direction in the first 30ms of the QRS. After that the speed shows no correlation with fiber directions, which means that the fiber directions of the epicardium have a dominant effect in the propagation of the wavefront only early after initial activation as reported in

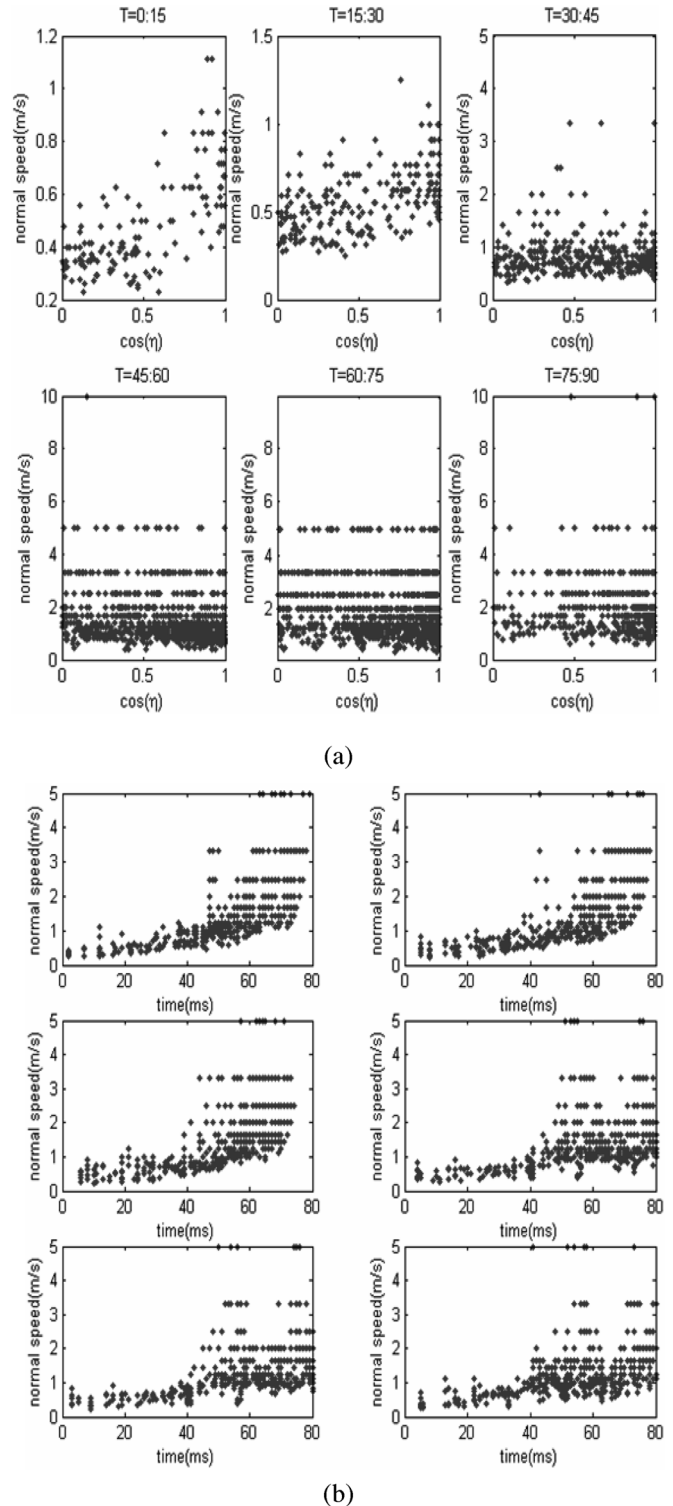


Fig. 2. (a) Speed normal to the wavefront versus cosine of angle between normal and local fibers (left ventricular pacing, time shown post pacing). (b) Speed normal to the wavefront versus time (left ventricular pacing, different sites).

[20] and [21]. Right ventricle paced beats showed similar results, but with reduced correlation between the speed and fiber directions, even early after initial activation, compared to left ventricle pacing.

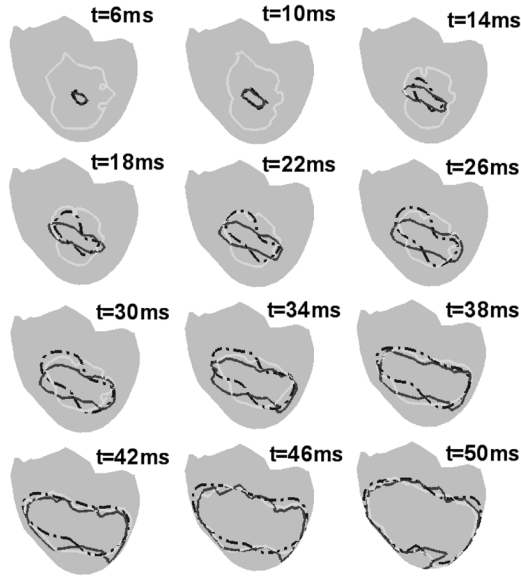


Fig. 3. Wavefront from experimental data (dark grey), Tikhonov solution (white) and WBCR approach (black, dashed line), t indicates the time with respect to the pacing in milliseconds.

Each panel of Fig. 2(b) shows the speed of the wavefront versus time during the QRS for a different left ventricle paced beat. We observed that the apparent speed of the wavefront generally increased over time. However, a high-speed wavefront was often observed in the middle of the QRS when the wavefront passed through one of three regions which showed consistently faster propagation: 1) the apex; 2) the mid and base regions of left ventricle; 3) the mid and base regions of right ventricle. In the region close to the intersection of the two ventricles (the septum), by contrast, speed was generally decreased. We observed similar results for the right ventricular paced beats.

These results provided the information needed to implement the WBCR approach, as explained in Section II-D. Fig. 3 shows the wavefront obtained from the experimental data (dark gray) along with the reconstructed wavefront using the WBCR method (black, dash line) and the wavefront obtained from a standard zero-order Tikhonov solution (white). The regularization parameters for the Tikhonov method were obtained from L-curves [30]. In all cases the wavefront was defined as the set of points whose potential equaled the average of the activated and inactive potential values. As can be seen in the figure, the proposed method was more accurate, especially for early activation times when the activated region was stretched along the local fiber directions.

B. Results of the WBPR Approach

Fig. 4 shows a potential map of an experimentally acquired left ventricular paced heartbeat, along with inverse solutions obtained by the WBPR approach (forward and backward), and the standard zero-order Tikhonov solution, at selected time instants. All the images in each row have the same mapping from value to gray shade and the contours show the iso-potential lines. The left column shows an electrogram from a point close to the pacing site on the heart. The time instant of each row is marked on the corresponding electrogram. The times shown beside the

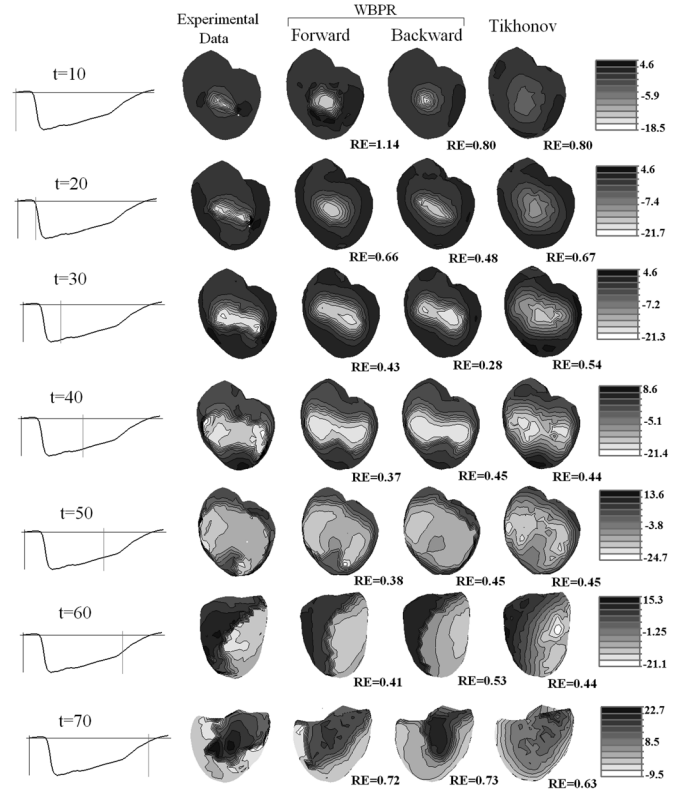


Fig. 4. Potential map of the experimental data along with the solutions of WBPR approach (forward and backward iteration) and Tikhonov for a left ventricular paced heartbeat. The parameter t shows the time in milliseconds with respect to the pacing. The left column shows the time signal of a point close to the pacing site. RE of each inverse solution is shown under corresponding potential map.

time signals represent the interval in milliseconds after pacing. The plots were drawn with *map3d* software [31]. We also calculated the relative error norm (RE) as $RE = \|\mathbf{x} - \hat{\mathbf{x}}\|/\|\mathbf{x}\|$, where \mathbf{x} and $\hat{\mathbf{x}}$ represent the experimental data and inverse solution, respectively. Fig. 6 shows the RE value versus time for the Tikhonov, WBPR forward and WBPR backward inverse solutions. The value of RE for each inverse solution at the selected time instants is also shown under corresponding potential map.

The results showed that reconstructed solutions using the proposed method were considerably improved over the Tikhonov solutions. As Fig. 4 shows, the backward iteration resolved the effect of errors in the initialization early after stimulus. At $t = 20$, the elliptical shape of the reconstructed wavefront was very similar to that of the experimental epicardial potentials. At all other time instants, the potential maps showed a sharp wavefront which was close to the position of the wavefront of the experimental epicardial potentials. At $t = 70$, the wavefront moved to the posterior side of the heart and the Tikhonov solution was quite smooth, while the solution from our forward iteration showed a wavefront location and potential map quite similar to the experimental data. Similarly, RE values as shown in Fig. 6 showed less error in the WBPR solutions than Tikhonov solutions, especially the backward WBPR in the first half of the QRS interval ($t < 35$) and forward WBPR in the second half ($t > 35$). However the RE values for $t > 63$ were larger for

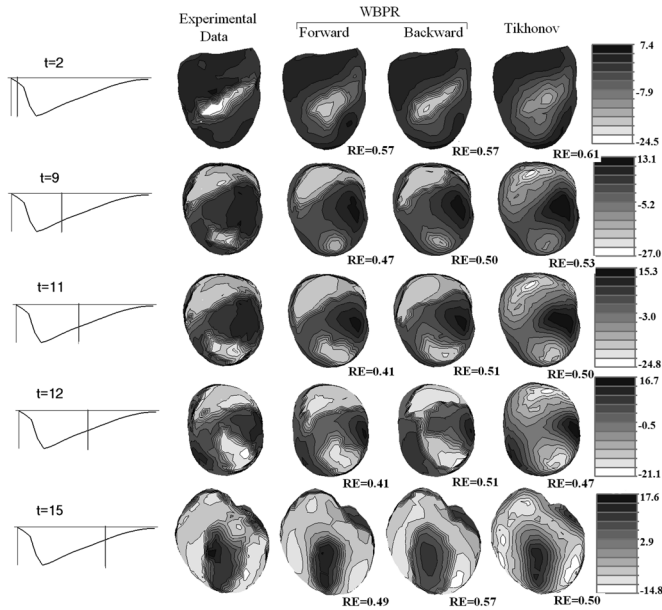


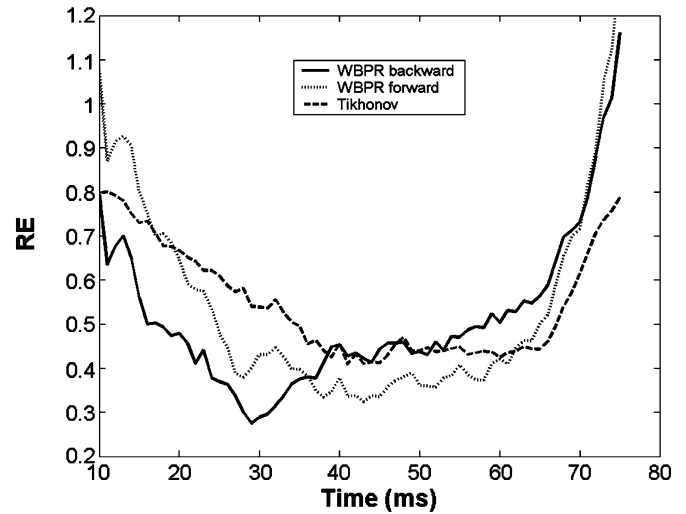
Fig. 5. Potential map of the experimental data along with the solutions of WBPR approach (forward and backward) and Tikhonov for an atrial drive paced heartbeat. The parameter t shows the time in milliseconds with respect to first breakthrough on the epicardial surface. The left column shows the time signal of a point close to the pacing site. RE of each inverse solution is shown under corresponding potential map.

WBPR approaches than Tikhonov despite the fact that the forward WBPR potential map reconstructed the wavefront location considerably more accurately than the Tikhonov solution.

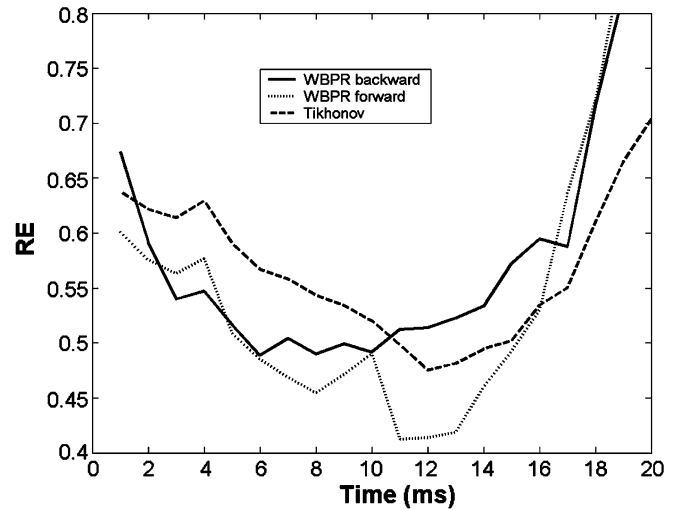
We also implemented our method for a supraventricularly stimulated beat to test its performance when multiple, separate activated regions were present on the heart surface. Fig. 5 shows potential maps at selected time instants of the experimental data along with the inverse solutions obtained by the WBPR approach (forward and backward) and by Tikhonov regularization. The times shown beside the time signals represent the interval in milliseconds with respect to the time that the first breakthrough appeared on the epicardium. At early time instants ($t = 2$), the potential map and wavefront location which were reconstructed by WBPR approach using a backward iteration compared quite accurately to the experimental data. Later on ($t = 9$), a second breakthrough appeared on the apex which the WBPR method was able to capture and represent more accurately than the Tikhonov solution. Three ms later ($t = 12$), the Tikhonov solution was very broad and smooth while the WBPR solutions much more clearly reflected the presence of a narrow wavefront, as found in the experimental data, and similarly at ($t = 15$). Interestingly, the RE figures for this latter time instant do not seem to predict this difference. The lower panel of Fig. 6 shows RE values as a function of time for this beat; again we note that the forward prediction method did better in the second half of QRS while the backwards method generally did better early in the beat only.

V. DISCUSSION

We have proposed two wavefront-based models in this paper. In the WBCR approach, we used a state-space formulation to solve the inverse problem of electrocardiography in terms of



(a)



(b)

Fig. 6. RE versus time (with respect to the pacing time) in milliseconds for (a) left ventricle paced and (b) supraventricular paced heartbeats.

the spread of activation on the epicardium. The basic motivation was to enable addition of physiological information about cardiac propagation to a low-dimensional, wavefront-based model. This information appeared in the state evolution function and wavefront-to-potential map of our state-space model. The use of the wavefront curve as the state variable (in contrast with earlier Kalman filtering approaches for inverse electrocardiography, which used the potentials as the state variable [32], [33]) both enforced the sharp transition across the wavefront and provided a low-dimensional and, therefore, potentially more robust, model. Moreover, the structure of the model facilitated our ability to include physiological properties of the heart such as fiber orientation. Results showed improvement with respect to the Tikhonov solution, especially at early times after the initial activation.

In the WBPR approach, the quantity of interest was the epicardial potential distribution. We exploited the relationship between the wavefront and epicardial potentials in the experimental data to construct a relatively simple potential model,

using an approximate wavefront curve to calculate an initial model of the potential. This initial estimate was then used to constrain the inverse solution in a deterministic Tikhonov method. One can equivalently consider this initial estimate as a mean value in a statistical Bayesian framework. In standard zero-order Tikhonov, this initial estimate (or the mean in the standard Bayesian approach) is assumed to be zero. We note that the WBPR approach applied the potential model constraint in a less strict way than the WBCR approach; the potential model used in the WBPR method is even simpler than that used in WBCR. We believe this approach is reasonable given that the WBPR method depends on this potential model in a much looser way than does the WBCR method.

The results of the WBCR approach illustrate a first step in building an appropriate model. We only used the fiber directions of the epicardial surface for our propagation model, while a more complete model should consider the 3-D effect of the fibers in the heart volume. We anticipate improvement by modifying $a(t)$, $b(t)$, and $\gamma(s)$ to reflect known behaviors like decline of the fiber direction effect in the speed function or increase of the wavefront speed at the apex. For instance, $\gamma(s)$ could be modeled as an appropriate piecewise constant function to reflect regions of higher and lower apparent speed, or $b(t)$ could be a non-decreasing function to reflect the general increase in apparent speed over time during a beat, as consistent with the experimental data. Moreover, one could build a potentially more accurate approach to model the potential surface by including at least some of the parameters of the potential model into the state variable. We note again that the fiber directions were approximated from a different canine heart than those used either for parameter determination or inverse solution testing, and that the geometry used for all the hearts at CVRTI was matched to a single generic model as well. Thus, our results suggest the relevance of using this prior information, even if not specific to a particular individual, to impose a spatio-temporal constraint on the wavefront behavior.

The filtering of the residual we employ in the WBCR method, to attenuate the effects of the error induced by our simplified, two-level, potential model, might well remove information which would be important in the solution of the inverse problem associated with a standard (high-dimensional) epicardial potential formulation. However our results suggest that this information is largely redundant in our low-dimensional, spatially and temporally constrained state-space model.

Results of the WBPR approach showed the importance of using the initial value in a deterministic Tikhonov framework (or in a Bayesian setting, the importance of using a non-zero estimate of the mean value). Considerable previous research in inverse electrocardiography has focused on using an appropriate covariance matrix (regularization matrix) to improve the inverse solution while the mean was assumed to be zero [34]. Some previous work which used an initial estimate of the solution to add temporal information used the smoothed Tikhonov solution [28]. It seems that such an approach did not effectively reflect the prior information that a wavefront exists. We tested the WBPR method with inclusion of a structured covariance matrix estimate (results not reported here), along with our structured estimate of the mean value; we estimated this covariance matrix

as a diagonal matrix whose diagonal elements were a function of the distance of corresponding nodes on the heart surface to the wavefront. The idea was that the initial estimate at the nodes farther from the wavefront should have less error than at the nodes closer to the wavefront and, thus, the diagonal elements of the error covariance matrix should be smaller for the nodes farther from the wavefront and larger for the nodes closer to the wavefront. However, somewhat surprisingly, our simulation results showed little improvement in the inverse solution when we used this covariance matrix to replace the simple model reported above of a scalar times the identity matrix. This suggests that previous neglect of the value of the mean in Bayesian approach may have been a source of considerable error.

One approach which could be considered would be to combine the mean estimator with a spatio-temporally derived estimate of the covariance matrix, for instance using an approach based on the isotropy assumption as proposed in [35]. The zero-order temporal predictor of the wavefront location in the current WBPR approach might also be improved by substitution of a more sophisticated model, such as the one used in the state evolution function of WBCR.

The backward iteration over time in the WBPR approach improved the inverse solution at early time instants after initial activation or breakthrough. At other time instants the solutions obtained by the backward iteration were sometimes worse than the solutions estimated in the forward iteration. However other methods of combining forward and backward iterations may result in further improvement.

In certain conditions, such as ischemia or postinfarction, the height of the wavefront changes on the heart. Activation-based methods tend to have difficulty with this problem, as noted in [11]. The WBCR approach is tied to simple propagation and potential models. To apply it to a wider range of conditions one would need to incorporate appropriate model parameters into the state variable, and then reconstruct them using torso potentials. Thus, a more complicated potential model than the one introduced in this work would be needed for this purpose. On the other hand, in the WBCR approach the effect of a predicted wavefront, as obtained by the evolution function, on the final estimated wavefront, is controlled by the prediction error. Therefore, wrong prior information increases the prediction error and as a consequence, this prediction has less effect on the final estimate. Another approach to increase applicability would be to design different speed functions for different conditions, and then choose among them based on corresponding prediction error, using a model invalidation method [36].

In contrast the WBPR approach does not impose a strictly determined wavefront height, as the WBCR approach does. In the current implementation of this method we found the wavefront from the estimated potentials by thresholding, assumed the wavefront curve was located at the mid-points of a fixed-height (20mv) wavefront transition region. Therefore, in conditions such as ischemia or postinfarction, careful attention may be required to the thresholding, and perhaps even an adaptive technique might need to be employed to detect the wavefront from the estimated potentials.

We point out that the results we presented here for the WBCR method were only qualitative; we did not compare the accu-

racy of the reconstructed curve to the wavefront in the original data in a quantitative fashion. Moreover, although we report RE values as a metric for assessing the accuracy of the WBPR method, as noted in Section IV the RE values at times did not correspond well to visual, i.e., qualitative, assessment of wavefront reconstruction, especially later in QRS. Examples are shown at time instants 50, 60, and 70 in Fig. 4 and time instants 12 and 15 in Fig. 5. We would have preferred to be able to include more meaningful quantitative metrics of accuracy. However we believe that meaningful quantitative comparison of wavefront curve location for WBCR, and more comprehensive accuracy of wavefront reconstruction in WBPR, requires the development and testing of new and appropriate metrics. There are many candidates in the literature for comparison of curves, which could be applied to results such as achieved by WBCR, but they have not been tested for applicability to cardiac wavefront location. Developing approaches for assessment of potential surfaces with wavefronts, such as reconstructed by WBPR, which take into account factors such as the extent and slope of the wavefront as well as its location, although certainly feasible, would require a significant degree of modification to existing metrics (whether of potential surfaces or wavefront curves).

In this study we used a forward model that only included the potentials on the epicardial surface. However the proposed methods are not limited to this setting and could be applied to models containing both epicardial and endocardial surfaces or transmembrane potential models [37]. The main change required in either method would be to build an appropriate geometric model and to substitute an appropriate wavefront-to-potential model.

VI. DIRECTIONS FOR FUTURE DEVELOPMENT

Our assumptions about the wavefront behavior and its relation with the epicardial potentials were based on epicardially paced beats. One goal of interest is to extend the methods to handle more complicated rhythms. Although we report here on promising results of a test of the WBPR approach on a supraventricularly paced beat, further testing and, most likely, development, are required. Beats with more than one wavefront curve can also be incorporated in the model used in the WBCR approach but represent a significant future challenge.

In our study, in order to concentrate on the performance of the methods without including additional complicating factors, we simulated the torso potentials from measured epicardial potentials without forward model error. This is clearly not a realistic setting for any kind of clinical or even experimental use. One might hope that our employment of a wavefront constraint and our careful estimation of the reference might indeed retain some of the robustness to this error shown by activation-based methods; however, this clearly needs to be investigated. Thus, a future study of interest will be to use more realistic data, such as from the outer surface of the CVRTI torso tank, with these methods. Another important area for future work is to study the robustness of the proposed methods against error in estimates of the reference drift and the initial activation node. Finally we plan to compare the accuracy of the inverse solutions obtained by these methods to that obtained by activation-based approaches.

ACKNOWLEDGMENT

The authors are indebted to B. Taccardi and B. Punske for their advice, encouragement, and critical comments on this work.

REFERENCES

- [1] C. Ramanathan, R. N. Ghanem, P. Jia, K. Ryu, and Y. Rudy, "Noninvasive electrocardiographic imaging for cardiac electrophysiology and arrhythmia," *Nature Med.*, vol. 10, pp. 422–428, 2004.
- [2] B. Tilg, G. Fischer, R. Modre, F. Hanser, B. Messnarz, M. Schocke, C. Kremser, T. Berger, F. Hintringer, and F. X. Roithinger, "Model-based imaging of cardiac electrical excitation in humans," *IEEE Trans. Med. Imag.*, vol. 21, no. 9, pp. 1031–1039, Sep. 2002.
- [3] J. J. M. Cuppen and A. van Oosterom, "Model studies with the inversely calculated isochrones of ventricular depolarization," *IEEE Trans. Biomed. Eng.*, vol. BME-31, pp. 652–659, 1984.
- [4] G. J. Huiskamp and A. van Oosterom, "The depolarization sequence of the human heart surface computed from measured body surface potentials," *IEEE Trans. Biomed. Eng.*, vol. 35, no. 12, pp. 1047–1059, Dec. 1989.
- [5] G. J. Huiskamp and F. Greensite, "A new method for myocardial activation imaging," *IEEE Trans. Biomed. Eng.*, vol. 44, no. 6, pp. 433–446, Jun. 1997.
- [6] A. J. Pullan, L. K. Cheng, M. P. Nash, C. P. Bradley, and D. J. Paterson, "Noninvasive electrical imaging of the heart: Theory and model development," *Ann. Biomed. Eng.*, vol. 29, pp. 817–836, 2001.
- [7] D. H. Brooks, G. F. Ahmad, R. S. MacLeod, and G. M. Maratos, "Inverse electrocardiography by simultaneous imposition of multiple constraints," *IEEE Trans. Biomed. Eng.*, vol. 46, no. 1, pp. 3–18, Jan. 1999.
- [8] F. Greensite and G. Huiskamp, "An improved method for estimating epicardial potentials from the body surface," *IEEE Trans. Biomed. Eng.*, vol. 45, no. 1, pp. 98–104, Jan. 1998.
- [9] A. van Oosterom, "The use of spatial covariance in computing pericardial potentials," *IEEE Trans. Biomed. Eng.*, vol. 46, no. 7, pp. 778–787, Jul. 1999.
- [10] C. Ramanathan, P. Jia, R. Ghanem, D. Calvetti, and Y. Rudy, "Noninvasive electrocardiographic imaging (ECGI): Application of the generalized minimal residual (GMRes) method," *Ann. Biomed. Eng.*, vol. 31, no. 8, pp. 981–994, Sep. 2003.
- [11] B. Messnarz, B. Tilg, R. Modre, G. Fischer, and F. Hanser, "A new spatiotemporal regularization approach for reconstruction of cardiac transmembrane potential patterns," *IEEE Trans. Biomed. Eng.*, vol. 51, no. 2, pp. 273–281, Feb. 2004.
- [12] C. Liu, G. Li, and B. He, "Localization of the site of origin of reentrant arrhythmia from body surface potential maps: A model study," *Phys. Med. Biol.*, vol. 50, no. 7, pp. 1421–1432, 2005.
- [13] R. Modre, M. Seger, G. Fischer, C. Hintermuller, D. Hayn, B. Pfeifer, F. Hanser, G. Schreier, and B. Tilg, "Cardiac anisotropy: is it negligible regarding noninvasive activation time imaging?," *IEEE Trans. Biomed. Eng.*, vol. 53, no. 4, pp. 569–580, Apr. 2006.
- [14] J. E. Burns, B. Taccardi, R. S. MacLeod, and Y. Rudy, "Noninvasive electrocardiographic imaging of electrophysiologically abnormal substrates in infarcted hearts: A model study," *Circulation*, vol. 101, pp. 533–540, 2000.
- [15] J. E. Burnes, B. Taccardi, and Y. Rudy, "A noninvasive imaging modality for cardiac arrhythmias," *Circulation*, vol. 102, pp. 2152–2158, 2000.
- [16] S. Ohyu, Y. Okamoto, and S. Kuriki, "Use of the ventricular propagated excitation model in the magnetocardiographic inverse problem for reconstruction of electrophysiological properties," *IEEE Trans. Biomed. Eng.*, vol. 49, no. 6, pp. 509–519, Jun. 2002.
- [17] L. K. Cheng, J. M. Bodley, and A. J. Pullan, "Effects of experimental and modeling errors on electrocardiographic inverse formulations," *IEEE Trans. Biomed. Eng.*, vol. 50, no. 1, pp. 23–32, Jan. 2003.
- [18] A. Ghodrati, D. H. Brooks, G. Tadmor, B. Punske, and R. S. MacLeod, "Wavefront-based inverse electrocardiography using an evolving curve state vector and phenomenological propagation and potential models," *Int. J. Bioelectromagnetism*, vol. 7, no. 2, pp. 210–213, 2000.
- [19] S. M. Kay, *Fundamentals of Statistical Signal Processing: Estimation Theory*. Upper Saddle River, NJ: Prentice-Hall, 1993.
- [20] B. Taccardi, R. L. Lux, P. R. Ershler, R. S. MacLeod, C. Zabawa, and Y. Vyhmeister, "Potential distributions and excitation time maps recorded with high spatial resolution from the entire ventricular surface of exposed dog hearts," in *Proc. Computers in Cardiology*, 1992, pp. 1–4.

- [21] B. Taccardi, E. Macchi, R. L. Lux, P. R. Ershler, S. Spaggiari, S. Baruffi, and Y. Vyhmeister, "Effect of myocardial fiber direction on epicardial potentials," *Circulation*, vol. 90, pp. 3076–3090, 1994.
- [22] B. Taccardi, R. L. Lux, R. S. MacLeod, P. R. Ershler, T. J. Dustman, M. Scott, Y. Vyhmeister, and N. Ingebrigtsen, "Electrocardiographic waveforms and cardiac electric sources," *J. Electrocardiol.*, vol. 29, pp. 98–100, 1996, (Suppl.).
- [23] F. Calderero, A. Ghodrati, D. H. Brooks, G. Tadmor, and R. MacLeod, "A method to reconstruct activation wavefronts without isotropy assumptions using a level sets approach," in *Proc. Functional Imaging and Modeling of the Heart 2005*, Barcelona, Spain, 2005, pp. 195–204.
- [24] P. M. Nielsen, I. J. LeGrice, B. H. Smaill, and P. J. Hunter, "Mathematical model of geometry and fibrous structure of the heart," *Am. J. Physiol.*, vol. 260, pp. 1365–1378, 1991.
- [25] B. P. Punske, R. L. Lux, R. S. MacLeod, P. R. Ershler, T. J. Dustman, Y. Vyhmeister, and B. Taccardi, "Experimental study and removal of the drift of the reference potential from the unipolar electrogram," in *Proc. 1st Joint BMES/EMBS Conf.*, 1999, p. 303.
- [26] B. Taccardi, S. Veronese, P. C. Franzone, and L. Guerri, "Multiple components in the unipolar electrogram: A simulation study in a three-dimensional model of ventricular myocardium," *J. Cardiovasc. Electrophysiol.*, vol. 9, no. 10, pp. 1062–1084, 1998.
- [27] B. B. Punske, Q. Ni, R. L. Lux, R. S. MacLeod, P. R. Ershler, T. J. Dustman, M. J. Allison, and Taccardi, "Spatial methods of epicardial activation time determination in normal hearts," *Ann. Biomed. Eng.*, vol. 31, no. 7, pp. 781–792, 2003.
- [28] H. S. Oster and Y. Rudy, "The use of temporal information in the regularization of the inverse problem of electrocardiography," *IEEE Trans. Biomed. Eng.*, vol. 39, no. 1, pp. 65–75, Jan. 1992.
- [29] R. S. MacLeod, Q. Ni, B. Punske, P. R. Ershler, B. Yilmaz, and B. Taccardi, "Effects of heart position on the body-surface ecg," *J. Electrocardiol.*, vol. S33, pp. 229–237, 2000.
- [30] P. C. Hansen, *Rank-Deficient and Discrete Ill-Posed Problems*. Philadelphia, PA: SIAM, 1997.
- [31] R. S. MacLeod and C. R. Johnson, "Map3d: Interactive scientific visualization for bioengineering data," in *Proc. IEEE Engineering in Medicine and Biology Society 15th Annu. Int. Conf.*, 1993, pp. 30–31.
- [32] J. El-Jakl, F. Champagnat, and Y. Goussard, "Time-space regularization of the inverse problem of electrocardiography," in *Proc. 17th Annu. IEEE-Engineering in Medicine and Biology Society Conf.*, 1995, pp. 213–214.
- [33] K. L. Berrier, D. C. Sorensen, and D. S. Khoury, "Solving the inverse problem of electrocardiography using a Duncan and Horn formulation of the Kalman filter," *IEEE Trans. Biomed. Eng.*, vol. 51, no. 3, pp. 507–515, Mar 2004.
- [34] A. van Oosterom, "The spatial covariance used in computing the pericardial potential distribution," in *Computational Inverse Problems in Electrocardiography*, P. R. Johnston, Ed. Southampton, UK: WIT, 2001, pp. 1–50.
- [35] F. Greensite, "The temporal prior in bioelectromagnetic source imaging problems," *IEEE Trans. Biomed. Eng.*, vol. 50, no. 10, pp. 1152–1159, Oct. 2003.
- [36] C. Mazzaro and M. Sznaier, "Robust Identification and Model (In)Validation of LPV Systems," in *Perspectives in Robust Control*. London, UK: Springer-Verlag, 2001.
- [37] B. Messnarz, M. Seger, R. Modre, G. Fischer, F. Hanser, and B. Tilg, "A comparison of noninvasive reconstruction of epicardial versus transmbrane potentials in consideration of the null space," *IEEE Trans. Biomed. Eng.*, vol. 51, no. 9, pp. 1609–1618, Sep. 2004.



Alireza Ghodrati received the B.Sc. degree in electrical engineering and the M.Sc. in biomedical engineering from University of Tehran, Tehran, Iran, in 1996 and 1999, respectively. He received the Ph.D. degree in electrical engineering from Northeastern University, Boston, MA, in 2005.

He is currently a Senior Project Engineer in the Algorithm Development Department, Draeger Medical, Andover, MA.



Dana H. Brooks (S'86–M'91–SM'06) received the B.A. degree in english from Temple University, Philadelphia, PA, in 1972 and the B.S.E.E., M.S.E.E., and Ph.D. degrees in electrical engineering from Northeastern University, Boston, MA, in 1986, 1988, and 1991, respectively.

He is Associate Professor of Electrical and Computer Engineering, Associate Director of the Center for Communications and Digital Signal Processing, and PI of the BioMedical Imaging and Signal Processing Laboratory, at Northeastern University, and

a member of the Center for Integrative Biomedical Computing headquartered at the University of Utah, Salt Lake City. He was a Visiting Professor during 1999–2000 at the Universitat Politècnica de Catalunya, Barcelona, Spain. His research interests lie in application of statistical and digital signal and image processing to biomedical signal processing and medical and biological imaging, and in open-source software systems for these applications.



Gilead Tadmor (M'87–SM'92) received the B.Sc. degree in mathematics from Tel Aviv University, Tel Aviv, Israel, in 1977 and the M.Sc. and Ph.D. degrees in mathematics (systems and control) from the Weizmann Institute of Science, Rehovot, Israel, in 1979 and 1984, respectively.

In 1989, he joined Northeastern University, Boston, MA, where he is a Professor of Electrical and Computer Engineering and the Director of the Communications and Digital Signal Processing Center for Research and Graduate Studies. He has

also held research, faculty and visiting positions at Tel Aviv University, Brown University, Providence, RI, the University of Texas, Dallas, the Laboratory for Information and Decision Systems at the Massachusetts Institute of Technology (M.I.T), Cambridge, SatCon Technology Corp., Boston, the Air Force Research Laboratory, Wright Patterson Air Force Base, OH, and the Technion, Haifa, Israel. His background is in the areas of robust and optimal control, distributed parameter systems, and mathematical systems theory. His recent active interests include robust and nonlinear control with applications in modeling and control of mechanical and fluid flow systems, dynamic imaging, and neural systems.



Robert S. MacLeod (S'87–M'87) received the B.S. degree in engineering physics and the Ph.D. degree in physiology and biophysics from Dalhousie University, Halifax, NS, Canada, in 1979 and 1990, respectively. He received the M.S. degree in electrical engineering from the Technische Universität, Graz, Austria, in 1985.

He is an Associate Professor in the Bioengineering Department and the Department of Internal Medicine (Division of Cardiology) at the University of Utah, Salt Lake City, and an Associate Director of the Sci-

entific Computing and Imaging Institute and the Nora Eccles Harrison Cardiovascular Research and Training Institute. His research interests include computational electrocardiography (forward and inverse problems), experimental investigation and clinical detection of cardiac ischemia and repolarization abnormalities, and scientific computing and visualization.